SPERRY FARRAGUT COMPANY

DIVISION OF SPERRY RAND CORPORATION
BRISTOL, TENNESSEE

MONTHLY TECHNICAL PROGRESS REPORT
DESIGN, DEVELOPMENT, AND FABRICATION
OF A REACTION WHEEL UTILIZING
A BRUSHLESS DC MOTOR

CONTRACT NO. NAS 5-9016

APRIL 1965

APPROVED BY:

J. M. WELCH
ENGINEERING DEPARTMENT HEAD

TO:

GODDARD SPACE FLIGHT CENTER
GREENBELT, MARYLAND

FROM:

SPERRY FARRAGUT COMPANY
DIVISION OF SPERRY RAND CORPORATION
BRISTOL, TENNESSEE

CONTENTS

ILLUSTRATIONS

SECTION I

INTRODUCTION

This is the tenth in a series of monthly technical progress reports covering the design, development, and fabrication of four reliable, efficient, lightweight, sealed brushless DC reaction wheel systems for Goddard Space Flight Center as described in Goddard Space Flight Center Specification No. 67-33 dated 4 March 1964 and Revision A dated 29 January 1965.

The reaction wheel is to be hermetically sealed for operation in hard-vacuum environments. It will be driven by a two-speed brushless DC motor with constant-torque limiting from 0 RPM up to 250 RPM and will have provision for varying the torque level by means of a DC control signal. Also, the motor is to provide a signal output proportional to speed. The goals for this program are described in detail in Goddard Specification No. 67-33, "Reaction Wheel with Electrically Commutated DC Torque Motor Drive," and in Revision A to this specification.

This report covers the reporting period from April 1 through April 30, 1965. The work performed during April consisted of:

1. Manufacturing effort on Units 1 and 2.

2. Motor and electronics development effort on Units 3 and 4.

SECTION II

FOREWORD

A. REACTION WHEEL SYSTEM (MECHANICAL)

    1. A test to compare the deflection of a flywheel with webs and a flywheel without webs was completed.

    2. Webs from flywheel No. 2 were removed. This resulted in an over-all weight reduction of .16 lbs. on flywheel.

B. BREADBOARD TEST (ELECTRICAL)

Design effort on Units 3 and 4 during this period was expended in the following areas:

    1. Tachometer design

    2. Commutator design

    3. Further development of regenerative braking circuits, including control circuitry.

    4. Incorporating bi-directional rotation when commanded by two separate 4 V DC signals.

    5. Photosensor mounting configuration for higher current output.

    6. An analysis of ripple torque caused by commutation was made for both a Delta winding configuration and a Wye winding configuration.

SECTION III

ENGINEERING AND LABORATORY EFFORTS

A. MECHANICAL STATUS

    1.   Flywheel Deflection Test (Reference Figure 1)

        A deflection test for comparison of a flywheel with webs and a flywheel without webs was made. The flywheels were statically loaded with weights up to 100 pounds and at this point the deflection of the flywheel without webs was 43 percent greater than the deflection of the flywheel with webs. Extension of the deflection lines to 375 pound load, as shown in Figure 1, indicates a deflection of .039 inches on the flywheel with webs and .054 inches on the flywheel without webs. This is approximately the same deflection that the flywheel would encounter during a 50 g shock.

    2.   Windage Test

        A windage test was completed on flywheels with and without webs. The data indicated that at 1/2 atmosphere there was no appreciable difference between the flywheel with webs and the flywheel without webs. The sealed units will be purged with 1/2 atmosphere of helium which will further minimize the difference. Removing the webs from the flywheel on Unit 2 reduced the weight by .46 pounds. An addition of inertia weight of .30 pounds is required to compensate for inertia loss from removal of webs. This will result in a weight saving of .16 pounds by removing webs.
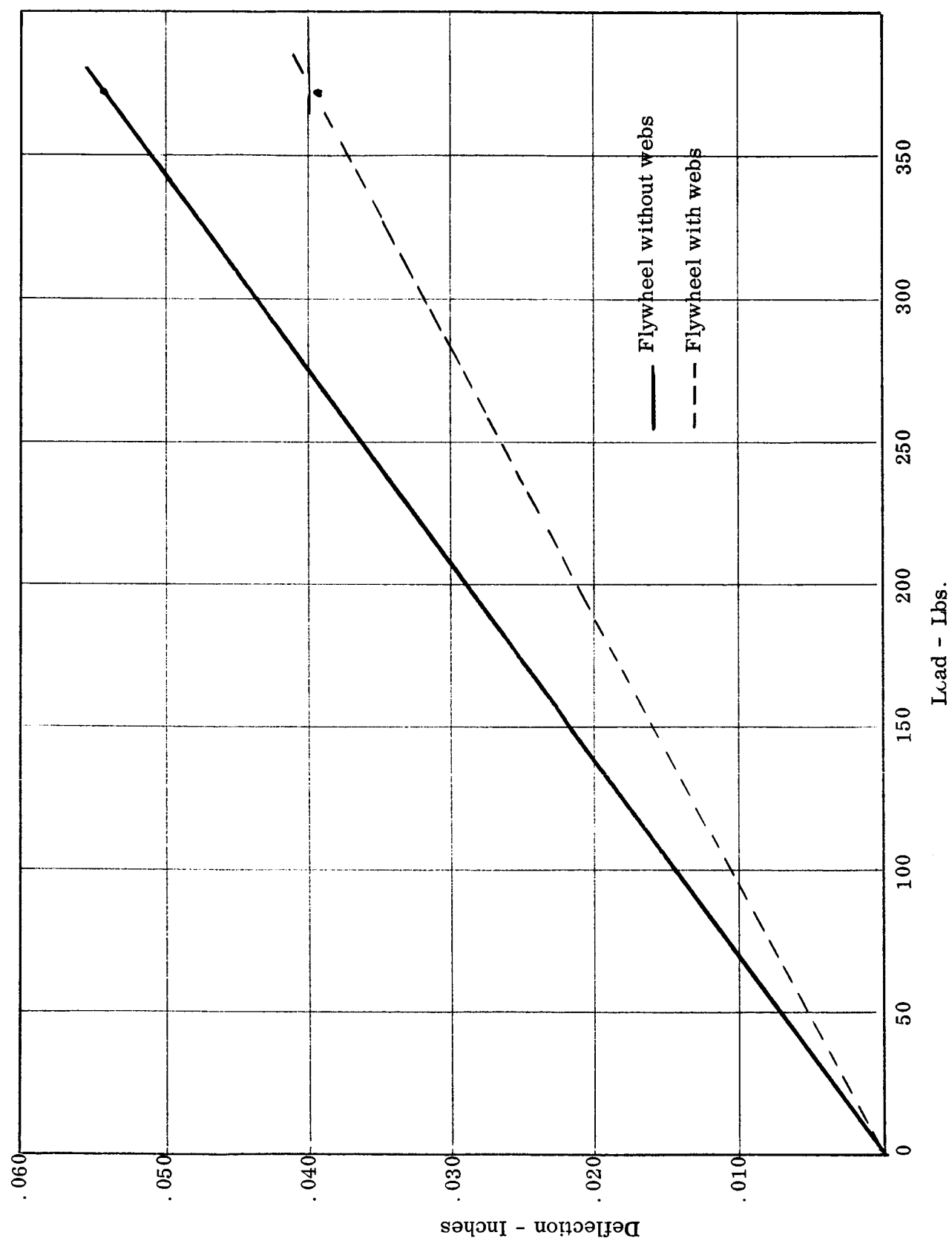
FIGURE 1
FIGURE DEFLECTION VS. LOAD

B.   MOTOR AND ELECTRONICS DEVELOPMENT

1.   Build Status (Units 1 and 2)

Unit 1 was delivered to Goddard Space Flight Center on 22 April 1965.
Assembly of Unit 2 is being delayed pending shipment of the cover and
housing from Piedmont Plating where they were sent to be black anodized.
The housing and cover are due to be shipped on 4 May.

Unit 1 was planned to be built with a non-skewed stator and Unit 2 was to
have a skewed stator.   However, earlier delivery of skewed stators than
was expected allowed Sperry Farragut to run torque ripple tests with both
stators and to prove that lower ripple was obtained with the skewed stator.
The skewed stator was then incorporated into Unit 1.   The torque ripple of
Unit 1 with the non-skewed stator was + 11.2% and -18.5%.   The ripple torque
with the skewed stator was +6.6% and -14.7%.   Figure 2 shows the torque ripple
of Unit 1.   Cogging torque was 0.029 ft. lbs. or ±5.8% of the total ripple torque.
Figure 3 is the speed torque curve for Unit 1.

The torque at 250 RPM is not 0.5 ft. lbs.   Part of the reason for this is that
at the time the stator winding was designed, it was known that a diode would
be required in series with each upper commutating switch.

The unit was run at -15°C and $+80^\circ$C but no torque measurements were made.
The Schmitt trigger which drives the tachometer and direction indicator
stopped operating at -13°C; however, the cause for this was not investigated.
Shock and vibration tests were not performed on Unit 1, nor were we able
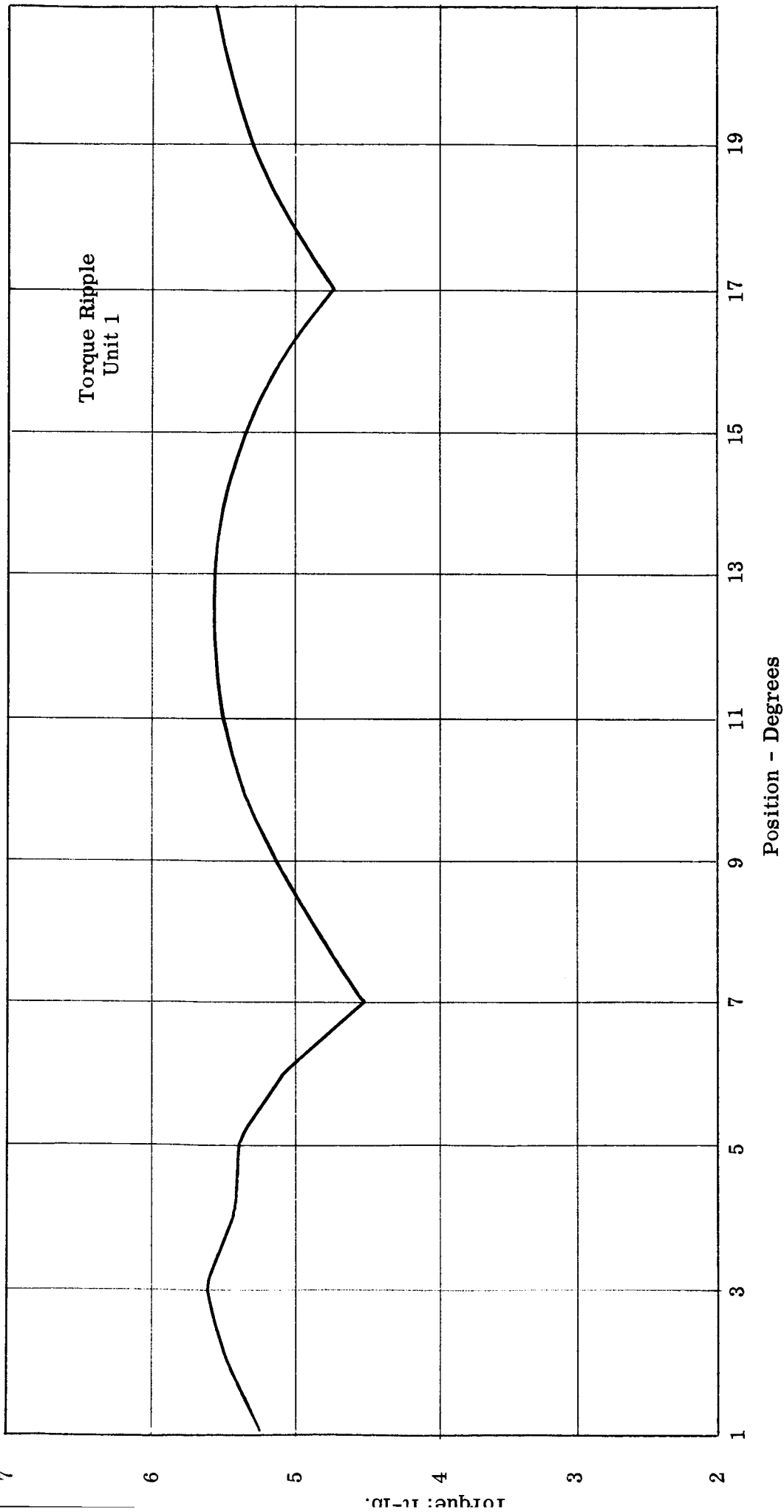to balance the flywheel on available equipment.   Provision has been made
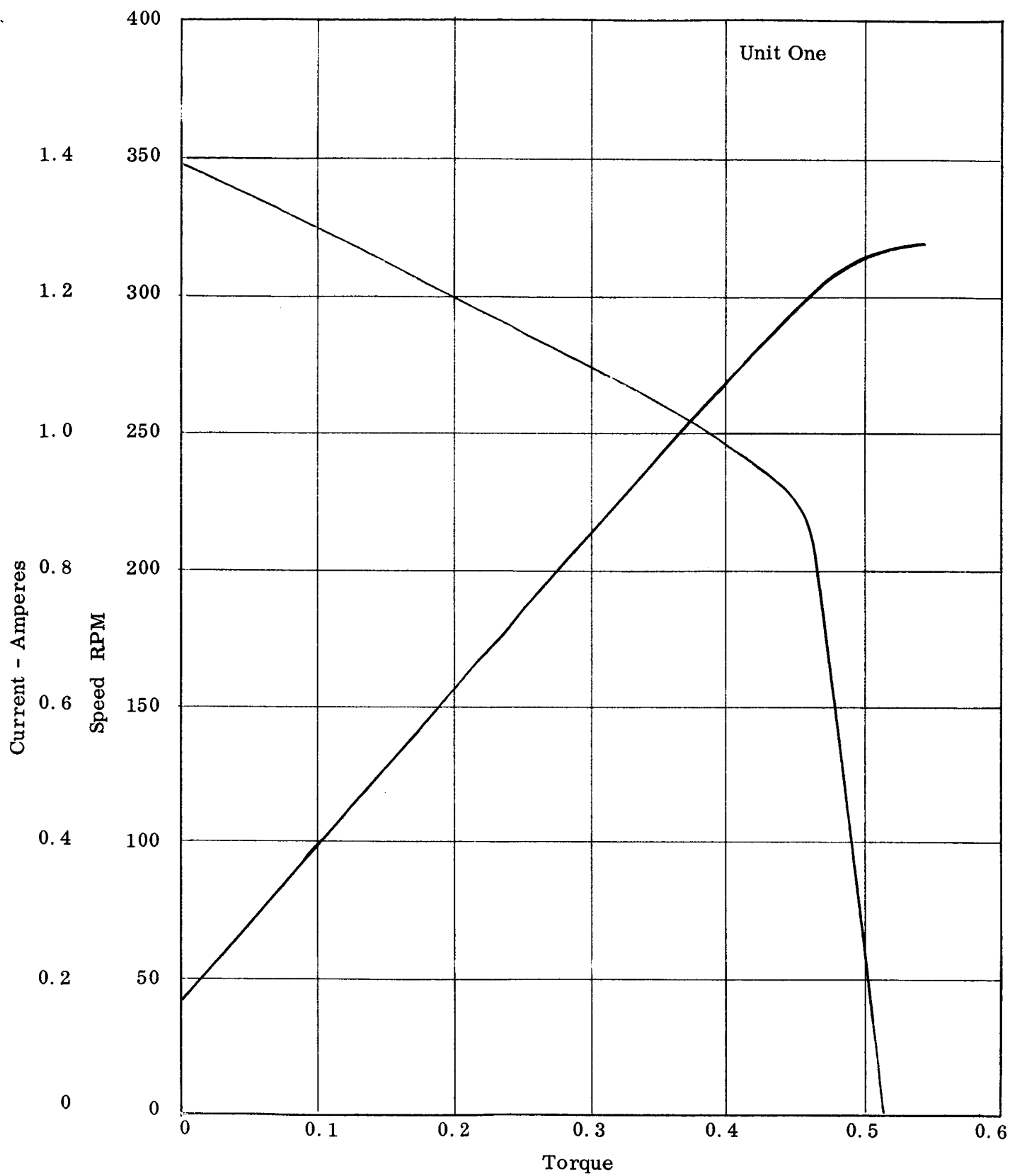
FIGURE 2
TORQUE RIPPLE

FIGURE 3
SPEED TORQUE CURVE

to statically balance the flywheel for Unit 2 and it will be shock tested and vibrated. Final measurements made at Sperry Farragut before delivery of Unit 1 showed a no-load current of 0.17 amperes at a speed of 337 RPM in both directions of rotation with the 250 RPM winding. With the 1000 RPM winding the no-load current was 0.83 amperes at a speed of 1250 RPM in both directions of rotation.

2. Commutation

The commutator for Unit 3 is shown in Figure 4. The components shown in dotted lines are those additional components necessary to incorporate regenerative braking. The commutator for Unit 4 will be the same as that for Unit 3 except for some resistance changes necessitated by lower current requirements of Unit 4. In Units 1 and 2 a diode was used in series with each upper switch to prevent breakdown of the upper switches when the motor was reversed. For units 3 and 4, the motor is to go into the regenerative braking mode where it will stay until the generated voltage is insufficient to provide the required current. Then the motor goes into the driving mode and at this time the generated voltage will be low enough that the output transistors in the upper switches will not break down. If the regenerative braking circuit ever failed, some protection might be required for the transistors, to insure that the motor could still perform satisfactorily. This protection was provided by replacing the upper switch Darlington resistor with a diode. Taking Switch 4, for example, this protects transistor Q3. To insure that the emitter-base junctions of Q2 and Q3 do not break down together, a diode CR3 and Zener diode CR4 were placed across Q3 to help keep the emitter of Q3 from going more than approximately 16 volts more positive than the collector. It would take approximately 22 volts to break down both junctions in series. The voltage divider action of R5 and R6 limits the voltage across each juntion to a safe value of approximately 7.5 volts.
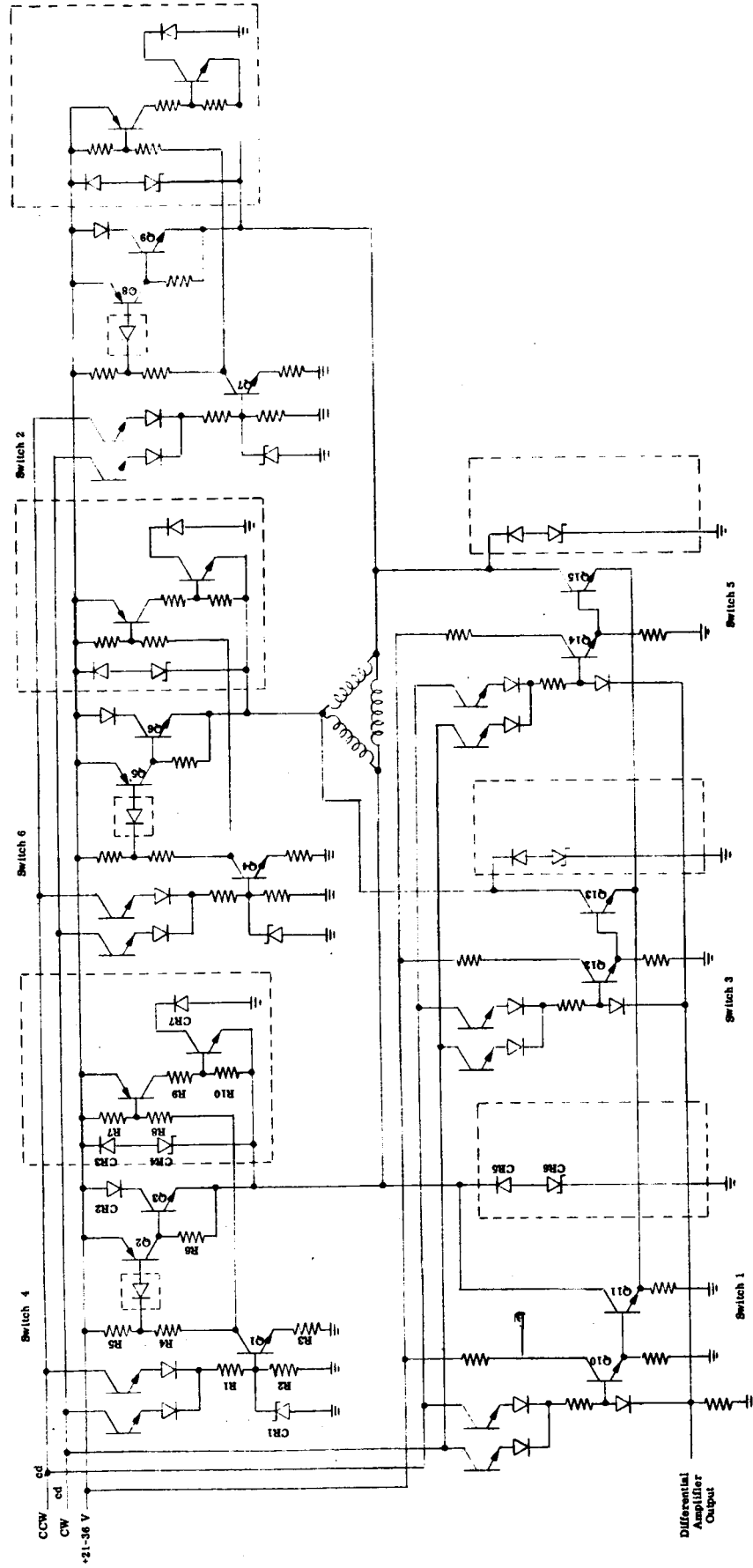
5
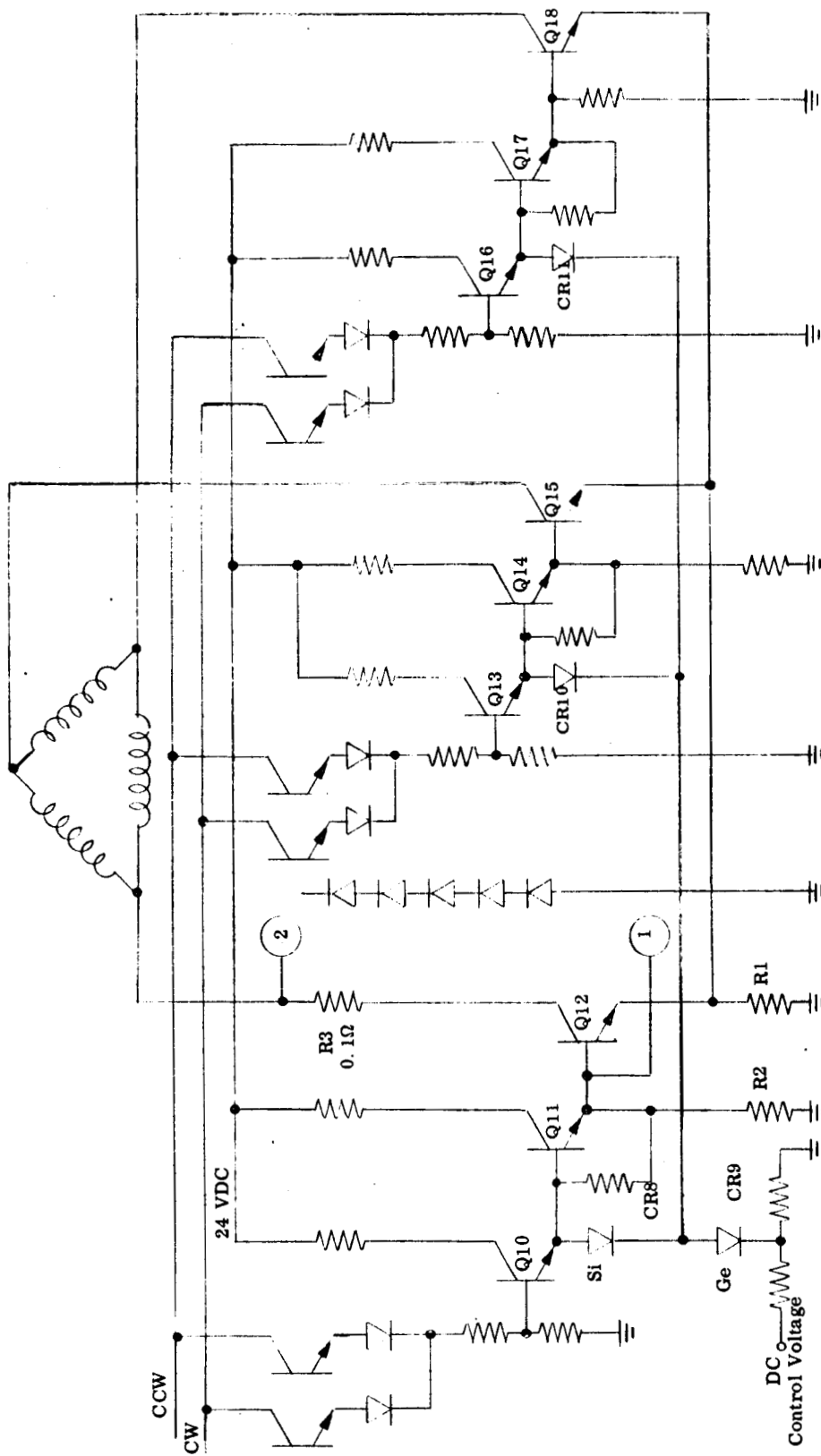
FIGURE 4
COMMUTATOR CIRCUIT FOR UNIT 3

FIGURE 5

CIRCUIT FOR INVESTIGATING CIRCULATING CURRENTS

3. Regenerative Braking

The circulating current problem discussed in previous progress reports was investigated further. With the lower switches connected as shown in Figure 5 current through the 0.1 ohm resistor was monitored as the motor was braking. It was found that the collector of Q12 was dropping to -12 volts and the base to -11.4 volts for a pulse time of about 1 millisecond, once per electrical cycle, while in the braking mode. When this negative voltage occurred, there was a reverse current through R3 of approximately 0.9 amps. With the circuit open at point 1, the same current still flowed. With the collector of Q12 open, a negative voltage pulse of -34 volts was observed. Transistor Q3 was experiencing zener breakdown and clipping the -34 pulse to -12 volts. The diode string shown in Figure 5 was placed from point 2 to ground. This stopped the breaking down of Q12, but the 0.9 amps was still flowing through R3. It was found that even with the diodes across Q12, the base of Q12 was still going far enough negative to cause the emitter of Q10 to go below ground and turn on. Since the emitter of Q12 is at approximately +1.25 volts, its collector at approximately -3.5 volts and its base at approximately -2.9 volts, it operates as a transistor and pumps current in the reverse direction. The emitter has now become the collector and the collector has become the emitter. By adding a resistor from the base to emitter of Q10, Q10 was prevented from turning on and the only base current available for Q12 was that allowed by R2, which is only a few milliamperes. The resulting configuration for the lower switches is that shown in Figure 4. The current limiting transistors are protected from breakdown and from conducting in the opposite direction. The only adverse effect caused by adding the diode and zener, CR5 and CR6, is that the 0.9 amperes mentioned above flows through the motor windings even though it does not go through the transistors in the reverse direction.

4. Bi-Directional Rotation

The circuit shown in Figure 6 provides a 24 volt supply to the appropriate set of photosensors upon receipt of a 4 V DC input. With no input command, Q16 and Q17 are both off. When an input command is applied to point 1, Q16 turns on and provides Q17 a base current path and causes Q17 to conduct. Q17 saturates and thus applies 24 V to the clockwise set of photosensors. CR7 is to prevent Q16 from turning on if some small leakage current flows into the base. If a command is applied to point 2, power is applied to the counter clockwise set of photosensors.

5. Lamp Tests

Tests were made to determine the mounting configuration and lamp voltage required to obtain sufficient sensor current to allow the removal of one stage of amplification in the lower switches. Maximum sensor output was obtained by letting the sensors look at the side of the lamp with a reflector (aluminum foil) behind the lamp. Table 1 shows the increase in sensor currents obtained by adding the reflector. Table 2 shows the sensor current obtained with a limiting resistor of 10 K and the voltage across each sensor. Indications are that the lamp will have to be operated with approximately 2.5 volts across it with a reflector, and at a distance of .050 inches from the sensor to provide the required current of approximately 2 ma and still have the sensors be saturated. The lamp voltage can be reduced if the distance between the lamp and the sensors can be lessened. The final mounting configuration and lamp voltage will depend to some extent upon what changes can be made to the lamp and sensor assemblies used on units one and two. However, these tests have proved that one stage of amplification can be removed from the lower switches. The breadboard system has been modified and is operating successfully with one stage of amplification removed.
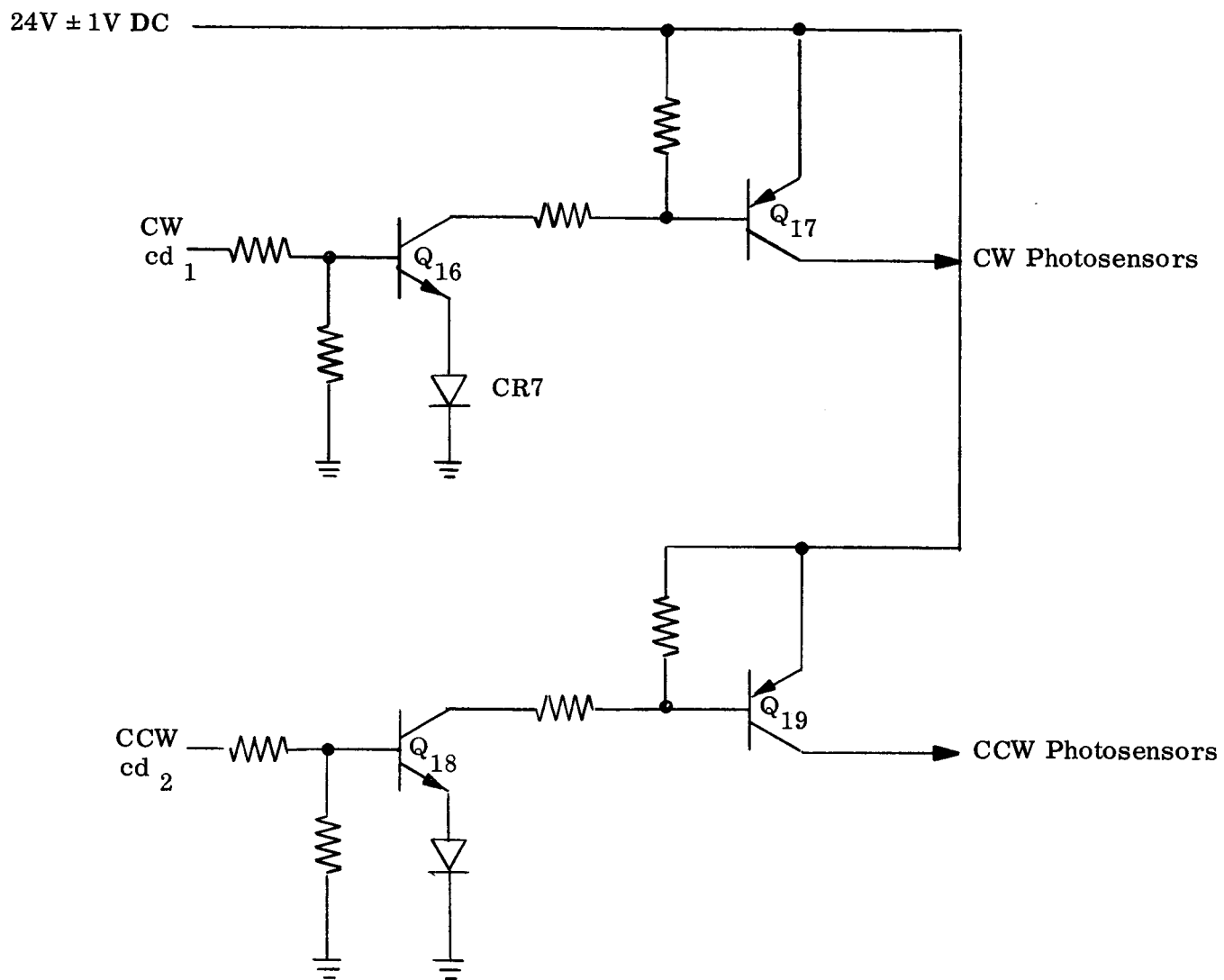
FIGURE 6
APPLICATION OF DIRECTION OF ROTATION COMMAND

TABLE 1

Distance between lamp and sensors = .050 inch

Limiting resistor = 5 K

Sensor Currents (MA)

Lamp Voltage	Without Reflector		With Reflector	
	Sensor 1	Sensor 2	Sensor 1	Sensor 2
2.0	0.36	0.3	1.3	0.9
2.5	0.97	0.82	3.4	2.3
2.8	1.58	1.25	4.5	3.4
3.0	2.0	1.74	4.5	4.35

TABLE 2

Distance between lamp and sensors = .050 inch

Limiting resistor = 10 K

Lamp Voltage	Current (MA)		Voltage	
	Sensor 1	Sensor 2	Sensor 1	Sensor 2
2.0	1.4	0.95	9.5	14
2.5	2.3	1.9	0.42	4.4
2.8	2.3	2.3	0.3	0.37

6. An analysis of torque ripple for both the Wye and Delta winding configurations was performed and is included in the appendix.

Tachometer

The tachometer circuit is a modified version of the configuration used on the first two reaction wheels.

The output voltage was increased from 2 volts to 10 volts at 250 RPM by increasing the time constant of the monostable multivibrator. The time constant increase was accomplished by increasing the coupling capacitor from .033 uf to .134 uf.

The maximum output voltage of the tachometer is 15.5 volts. Without compensation, this occurs at approximately 400 RPM. At this point the monostable is being operated at its maximum repetition rate. A further increase in the trigger rate results in the monostable triggering on alternate pulses which drops the output voltage to approximately 8 volts.

Since the maximum no-load speed of the reaction wheel (Unit 3) is near 400 RPM, compensation was added to the tachometer to prevent the maximum repetition rate from being exceeded. A 21 volt Zener diode was added to provide feedback from the tachometer output to the base of the monostable output transistor to reduce the time period. The feedback occurs only when the output is above 10 volts so that the output linearity from 0 to 10 volts is not disturbed. With feedback, the maximum repetition rate occurs at 600 RPM, a value the reaction wheel will not reach. A Zener with a breakdown voltage of 19 to 20 volts would probably result in an increase in linearity since its feedback effect would decrease the tachometer output at a lower speed. When the tachometer output is near 10 volts, the value is higher than it would be if it was completely linear, refer to Figure 7.

The output impedance of the tachometer is 8 K ohms. By using an emitter follower output stage, the output impedance is reduced to less than 100 ohms. Both the tachometer circuit and the emitter follower stage are shown in Figure 8.
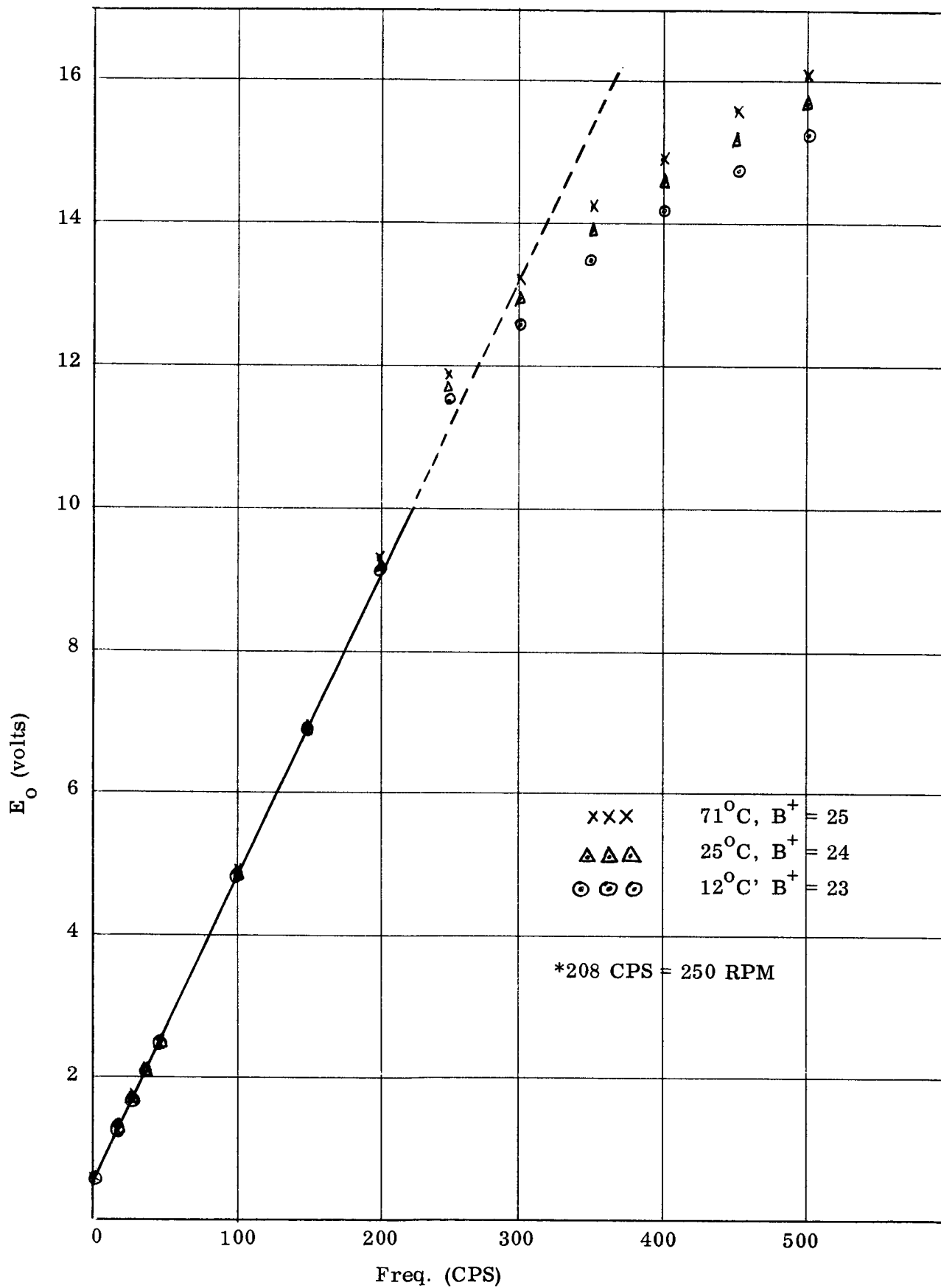
9

FIGURE 7
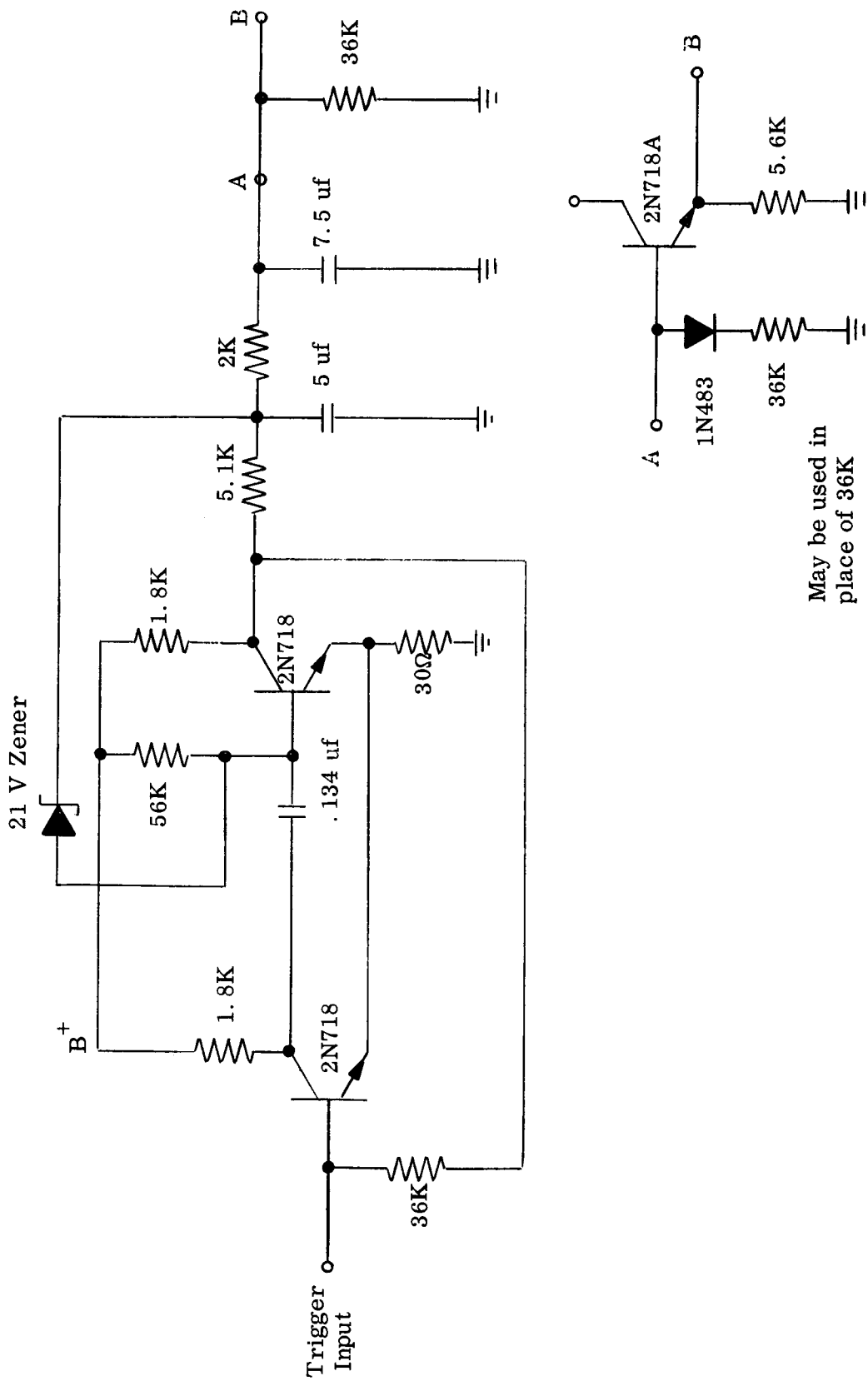TACHOMETER OUTPUT – TEMPERATURE AND B^+ EXTREMES

FIGURE 8
TACHOMETER CIRCUIT

Tachometer output voltage under voltage and temperature extremes is shown in Figure 7. Approximately 1% of the variation is caused by the power supply change, the remainder is due to the temperature variation.

The transistors in the monostable multivibrator produce the largest amount of the tachometer output voltage variation with temperature. The use of a temperature compensated capacitor in the monostable reduces the variation due to this component to a negligible amount.

A spot check using the diode compensated emitter follower output stage indicated a negligible amount of added drift.

SECTION IV

ADMINISTRATIVE STATUS

A. SCHEDULE

The first motor under this contract was shipped on 21 April 1965. The

expected delivery date for the second unit is 1 June 1965. This prediction

reflects a delay from the previous forecast of 7 May 1965 caused by a

vendor's plating problems on three critical parts.

The remaining two motors will be built to a modified design. The new design

is presently on machining and assembly hold awaiting the new engineering release.

B. FUNDING

At the present time it appears that the Sperry Farragut costs will equal or

exceed the total dollars including fee proposed in our letter 23-65-0402 dated

15 March 1965.

AN ANALYSIS OF COMMUTATION TORQUE
PULSATION IN A BRUSHLESS DC MOTOR

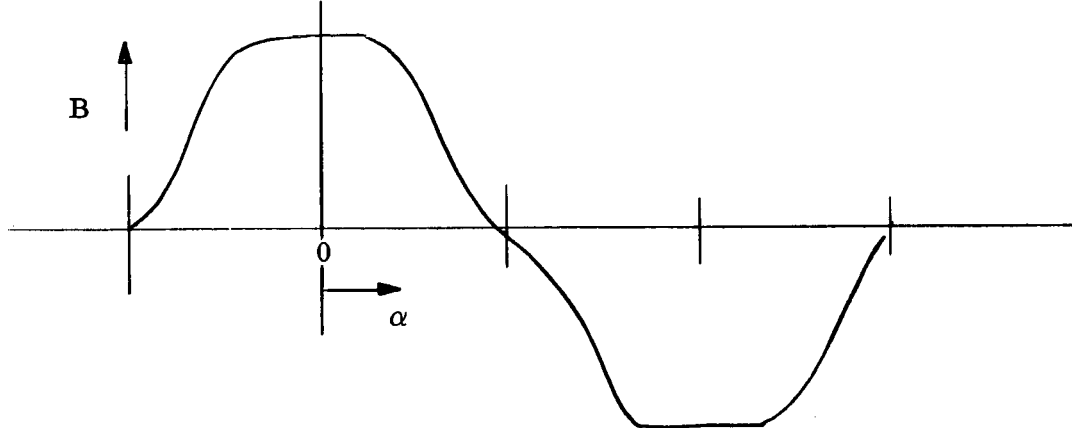The flux distribution in the air gap of a typical brushless DC motor appears approximately as shown in Figure A1.

FIGURE A1
AIR GAP FLUX DISTRIBUTION IN A TYPICAL BRUSHLESS DC MOTOR

This distribution is characterized by a flattening of the wave crest as a result of saturation in portions of the rotor or stator. In general the flux distribution may be expressed as a Fourier series of the form

$$\textcircled{1} \quad B\,(\alpha) = \sum_{n=1}^{\infty} B_n \cos n\alpha \quad \text{gauss}$$

where the B_n coefficients may be determined from search coil or flux meter measurements. By symmetry, the wave will contain only odd order harmonics.

The armature of a typical BDCM is wound with chorded, distributed coils which respond primarily to the fundamental component of flux distribution and produce an induced or counter EMF that is essentially a sinusoidal function of time. This is objectionable in a brushless motor that uses only six commutating zones per pair of

poles because the counter EMF pulsates between 86.6% and 100% of its peak value during each commutating period. The pulsations in EMF cause similar pulsations in current and in torque and the motor exhibits a commutation cogging or ripple effect.

The commutation cogging effect would be eliminated or attenuated if the armature winding responded to some or all of the air gap flux harmonics such that the counter EMF would be essentially constant over the commutating zone. This is theoretically possible to achieve, however, there are obstacles and limitations which will be revealed in the following analysis.

A typical brushless DC motor uses only six commutating zones for reasons of size, weight, economy and reliability. Six commutating zones are associated with three armature winding terminals and three identical phase windings which must be connected in either a delta or a wye configuration.

Figure A2 represents a simple two pole motor with three concentrated, full pitch phase windings.
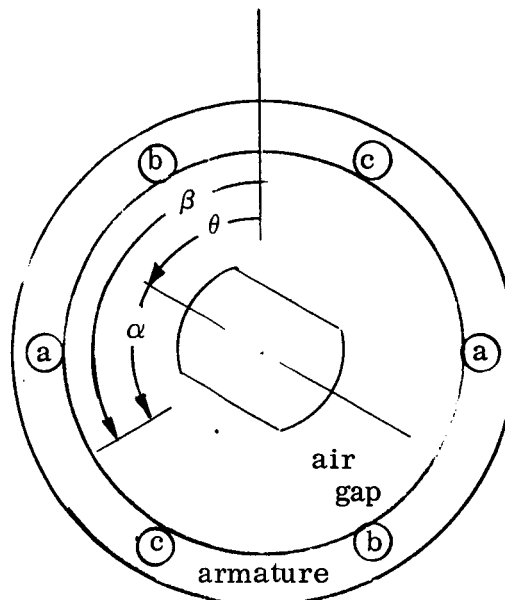

FIGURE A2
SIMPLE TWO POLE MOTOR

In Figure A2 –

α = a mechanical angle measuring distance around the air gap from a
rotor reference axis.

β = a mechanical angle measuring distance around the air gap from an
armature reference axis.

θ = the rotor position angle and from Figure A2

$$\textcircled{2} \quad \beta = \alpha + \theta$$

It will be assumed that the air gap flux distribution is of the most general form and
is given by equation 1 which may be referred to the armature by equation $\textcircled{2}$.

$$\textcircled{3} \quad B(\beta) = \sum_{n=1}^{\infty} B_n \cos[n(\beta - \theta)] \quad \text{gauss.}$$

If the radius to the air gap is (r) and the axial length of the gap is (l), the flux linking
phase (a) of Figure A2 is

$$\textcircled{4} \quad \phi_a = rl \int_{-\frac{\pi}{2}}^{+\frac{\pi}{2}} B(\beta)\, d\beta = 2\,rl \sum_{n=1}^{\infty} \frac{B_n}{n} \sin n \frac{\pi}{2} \cos n\,\theta \quad \text{maxwells.}$$

Assume that the rotor turns at a speed $\omega = \dfrac{d\theta}{dt}$. The EMF induced in phase (a) is then –

14

$$\text{(5)} \quad e_a = -N \frac{d\phi_a}{dt} = -\omega N \frac{d\phi_a}{d\theta} = 2\omega r l N \sum_{n=1}^{\infty} B_n \sin n\frac{\pi}{2} \sin n\theta$$

$$\text{or} \quad e_a = \sum_{n=1}^{\infty} E_n \sin n\frac{\pi}{2} \sin n\theta \quad \text{abvolts}$$

$$\text{where} \quad E_n = 2\omega r l N B_n$$

Similarly, the voltages induced in phases (b) and (c) are –

$$\text{(6)} \quad e_b = \sum_{n=1}^{\infty} E_n \sin n\frac{\pi}{2} \sin\left[n\left(\theta - \frac{2\pi}{3}\right)\right]$$

$$e_c = \sum_{n=1}^{\infty} E_n \sin n\frac{\pi}{2} \sin\left[n\left(\theta + \frac{2\pi}{3}\right)\right] \quad \text{abvolts}$$

Figure A3 represents a delta connection of the three phases where (R) is the resistance per phase and (i) is a current that circulates in the delta.
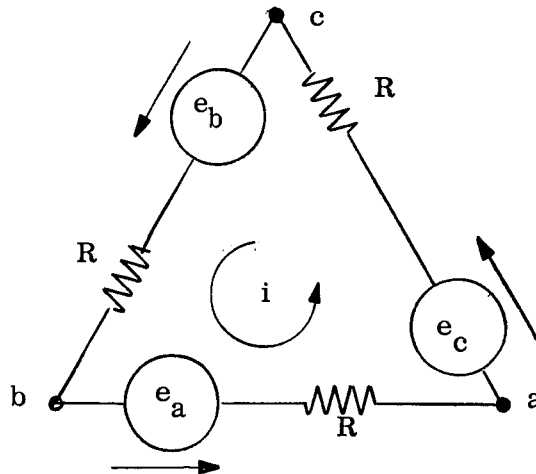

FIGURE A3
DELTA CONNECTION

The voltage loop equation for the delta is -

$$\text{(7)} \quad 3Ri = e_a + e_b + e_c = \sum_{n=1}^{\infty} E_n \sin n \frac{\pi}{2} \left[1 + 2\cos\frac{2n\pi}{3}\right] \sin n\theta$$

and the open circuit voltage across terminals (ba) is -

$$\text{(8)} \quad e_{ba} = e_a - Ri = \frac{4}{3} \sum_{n=1}^{\infty} E_n \sin n \frac{\pi}{2} \sin^2 \frac{2n\pi}{3} \sin n\theta$$

$$\text{or} \quad e_{ba} = E_1 \sin\theta + E_5 \sin 5\theta - E_7 \sin 7\theta - E_{11} \sin 11\theta + - - - -$$

The terminal voltage wave shape is not the same as the flux wave because all third order harmonics are absent. The alternate wye connection of Figure A4 may also be examined.
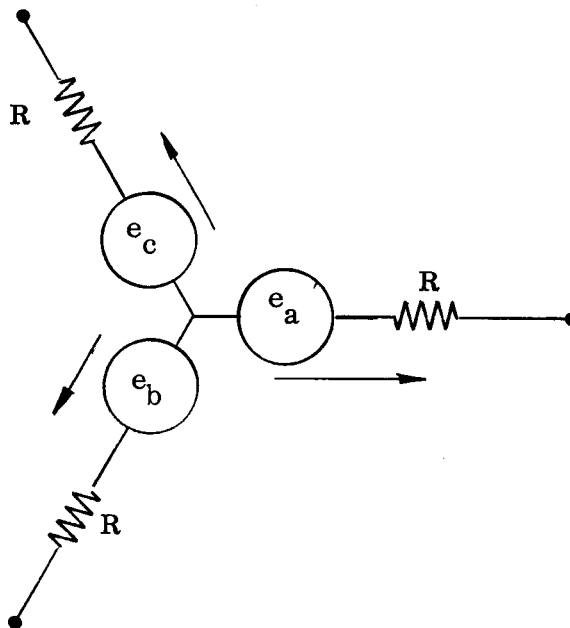

FIGURE A4
WYE CONNECTION

16

There is no circulating current in the wye and the open circuit voltage across two terminals (b and c) is -

$$\text{(9)} \quad e_{bc} = e_c - e_b = 2 \sum_{n=1}^{\infty} E_n \sin n \frac{\pi}{2} \sin \frac{2n\pi}{3} \cos n\theta$$

$$\text{or} \quad e_{bc} = \sqrt{3} \left[E_1 \cos \theta - E_5 \cos 5\theta - E_7 \cos 7\theta + E_{11} \cos 11\theta + - - - \right]$$

The third harmonic is also absent from the wye connection, in fact, this is a fundamental characteristic of all three phase windings regardless of how the windings are chorded and distributed.

The third harmonic has the most pronounced effect toward flattening the crest of a wave and its absence from the terminal voltages of both the delta and wye windings removes an opportunity for obtaining a voltage that is relatively constant over the commutating zone. This restriction can be removed by using a five phase winding, but this is objectionable for the reasons mentioned earlier.

In spite of the absence of the third harmonic from three phase terminal voltages it may still be possible to obtain some flattening of the EMF wave by utilizing the fifth and higher order flux harmonics provided that these harmonics exist and are of suitable amplitude and polarity. A general analysis of this approach including all possible variables would lead to enormous mathematical complications. To demonstrate the principle and examine its feasibility a simple case using only the fifth harmonic will be considered.

17

A voltage wave having the form -

(10) $\quad e = [\sin\theta - k\ \sin 5\ \theta]$

or $\quad e = [\cos\theta - k\ \cos 5\ \theta]$

would be depressed at its peak and would have less variation over the commutating zone than a sinusoidal voltage. It has been determined that a 7% fifth harmonic content (k = .07) gives a wave which varies in amplitude by only 2.6% over the 60 degree commutating zone as compared to 13% for a sine wave. To make use of equation (10) it is necessary to devise an armature winding that will respond strongly to the fifth harmonic of flux in addition to a normal response to the fundamental component.

The response of an armature coil to a given flux harmonic is proportional to its pitch factor, which is given by -

(11) $\quad C_n = \sin\ n\ \dfrac{\beta_0}{2}$

where β_0 is the span of the coil in electrical radians. For maximum response to the fifth flux harmonic -

(12) $\quad C_5 = \sin\ \dfrac{5\beta_0}{2} = \pm 1$

or $\quad \beta_0 = \dfrac{\pi}{5},\ \dfrac{3\pi}{5},\ \pi,$ etc.

18

An armature with 10 slots per pair of poles or a multiple of 10 slots would provide the required coil pitch, but since the number of slots should also be a multiple of 3 for a 3 phase winding the armature would require 30 slots per pair of poles. This is impractical and as a compromise an armature with 9 slots per phase will be considered. Figure A5 represents a 2 pole, 9 slot armature in which only one phase winding is shown.
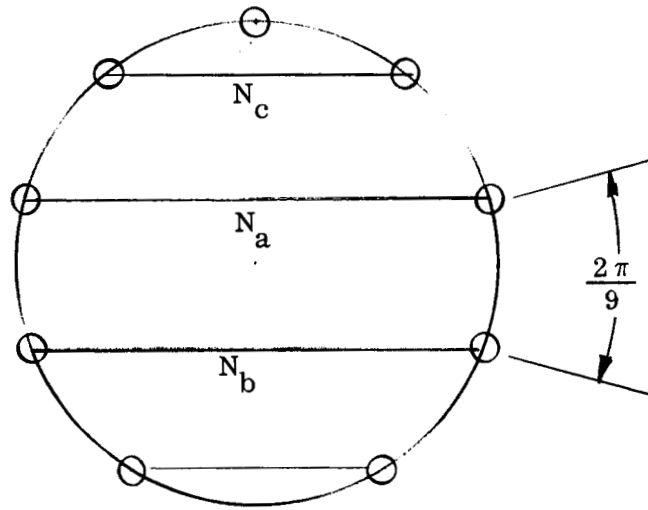

FIGURE A5
2 POLE, 9 SLOT ARMATURE

A 9 slot armature will accommodate 3 coils per phase represented by N_a, N_b and N_c. The fundamental and fifth harmonic pitch factors for these coils are -

(13) $\quad C_{a1} = \sin \frac{4\pi}{9} = .985 \qquad\qquad C_{a5} = \sin \frac{2\pi}{9} = .643$

$\qquad C_{b1} = \sin \frac{\pi}{3} = .866 \qquad\qquad C_{b5} = -\sin \frac{\pi}{3} = -.866$

$\qquad C_{c1} = \sin \frac{2\pi}{9} = .643 \qquad\qquad C_{c5} = -\sin \frac{\pi}{9} = -.342$

Coil N_c does not respond well to either the fundamental or fifth harmonic of flux and it will be omitted for better utilization of slot winding space.

In general the air gap flux distribution will be –

$$(14) \quad B(\beta) = \sum_{n=1}^{\infty} B_n \cos[n(\beta - \theta)] \quad \text{gauss}$$

The flux linkages with coil N_a are –

$$(15) \quad \Psi_1 = N_a \phi_1 = rlN_a \int_{-\frac{4\pi}{9}}^{+\frac{4\pi}{9}} B(\beta) \, d\beta = 2rlN_a \sum_{n=1}^{\infty} \frac{B_n}{n} \sin \frac{4n\pi}{9} \cos n\theta$$

maxwell - turns

and the EMF induced in N_a is –

$$(16) \quad e_1 = -\omega \frac{d\Psi_1}{d\theta} = 2\omega rlN_a \sum_{n=1}^{\infty} B_n \sin \frac{4n\pi}{9} \sin n\theta \quad \text{abvolts}$$

Similarly, the EMF induced in coil N_b is –

$$(17) \quad e_2 = 2\omega rlN_b \sum_{n=1}^{\infty} B_n \sin \frac{2n\pi}{3} \sin n\theta \quad \text{abvolts}$$

The phase voltage is the sum of the individual coil voltages, hence for phase (a) –

$$(18) \quad e_a = e_1 + e_2 = 2\omega rl \sum_{n=1}^{\infty} B_n N_n \sin n\theta$$

where

$$(19) \quad N_n = N_a \sin \frac{4n\pi}{9} + N_b \sin \frac{2n\pi}{3} \quad \text{effective turns}$$

20

The voltages induced in phases (b) and (c) are

(20) $e_b = 2\omega r l \sum_{n=\pi}^{\infty} B_n N_n \sin[n(\theta - \frac{2\pi}{3})]$

$e_c = 2\omega r l \sum_{n=1}^{\infty} B_n N_n \sin[n(\theta + \frac{2\pi}{3})]$

The resultant delta and wye connected terminal voltages are -

(21) $e_\Delta = \frac{8}{3} \omega r l \sum_{n=1}^{\infty} B_n N_n \sin^2 \frac{n\pi}{3} \sin n\theta$

or $e_\Delta = 2\omega r l B_1 N_1 [\sin\theta + \frac{B_5 N_5}{B_1 N_1} \sin 5\theta + - - - -]$

(22) $e_y = 4\omega r l \sum_{n=1}^{\infty} B_n N_n \sin \frac{2n\pi}{3} \cos n\theta$

or $e_y = 2\sqrt{3} \omega r l B_1 N_1 [\cos\theta - \frac{B_5 N_5}{B_1 N_1} \cos 5\theta + - - - -]$

If only the first two terms of each series are considered the voltages may be put in the form of equation (10) where -

(23) <u>Δ winding</u>   <u>y winding</u>

$E = 2\omega r l B_1 N_1$ $E = 2\sqrt{3} \omega r l B_1 N_1$

$k = - \frac{B_5 N_5}{B_1 N_1}$ $k = \frac{B_5 N_5}{B_1 N_1}$

$(k = .07)$

21

Substituting from equation ⑲ leads to two simultaneous equations in N_a and N_b. In the case of the delta winding the coil turns are

$$\text{㉔} \quad N_a \bigg|_\Delta = \frac{E(B_5 - kB_1)}{4\omega r l B_1 B_5 \sin\frac{\pi}{3} \cos\frac{\pi}{9}}$$

$$N_b \bigg|_\Delta = \frac{E(B_5 + 2kB_1 \cos\frac{2\pi}{9}) \sin\frac{\pi}{9}}{2\omega r l B_1 B_5 \sin^2\frac{\pi}{3}} \quad \text{turns}$$

and the ratio of these turns for k = .07 is

$$\text{㉕} \quad \frac{N_a}{N_b} \bigg|_\Delta = 1.35 \left[\frac{\frac{B_5}{B_1} - .07}{\frac{B_5}{B_1} + .107} \right]$$

Equations ㉔ and ㉕ may be converted for the wye winding by reversing the sign of (k) and introducing the factor $\sqrt{3}$. Equation ㉕ becomes –

$$\text{㉖} \quad \frac{N_a}{N_b} \bigg|_y = 1.35 \left[\frac{\frac{B_5}{B_1} + .07}{\frac{B_5}{B_1} - .107} \right]$$

In the fully wound armature the N_a coils occupy a full slot per coil side and the N_b coils share a slot. For optimum utilization of slot space the ratio of turns should be 2. From equations ㉕ and ㉖ this requires –

22

(27) $\left.\dfrac{B_5}{B_1}\right|_{\Delta}$ $= -.4746$ $\qquad$ $\left.\dfrac{B_5}{B_1}\right|_{y}$ $= +.4746$

$$\text{for } \left|\frac{N_a}{N_b}\right| = 2$$

In practice the ratio of the flux coefficients is more or less an accident of design and it is either impossible or very difficult to achieve an exact flux distribution. In order to determine if either of the conditions of equation (27) can be achieved, the typical air gap flux distribution of Figure A1 will be approximated by a trapezoidal wave as shown in Figure A6.
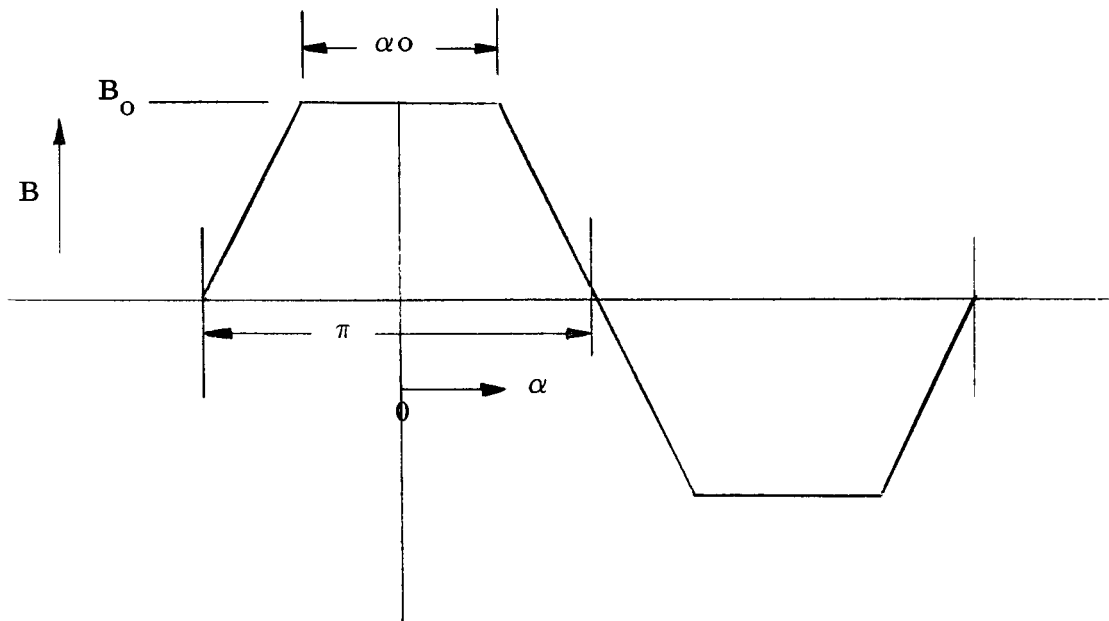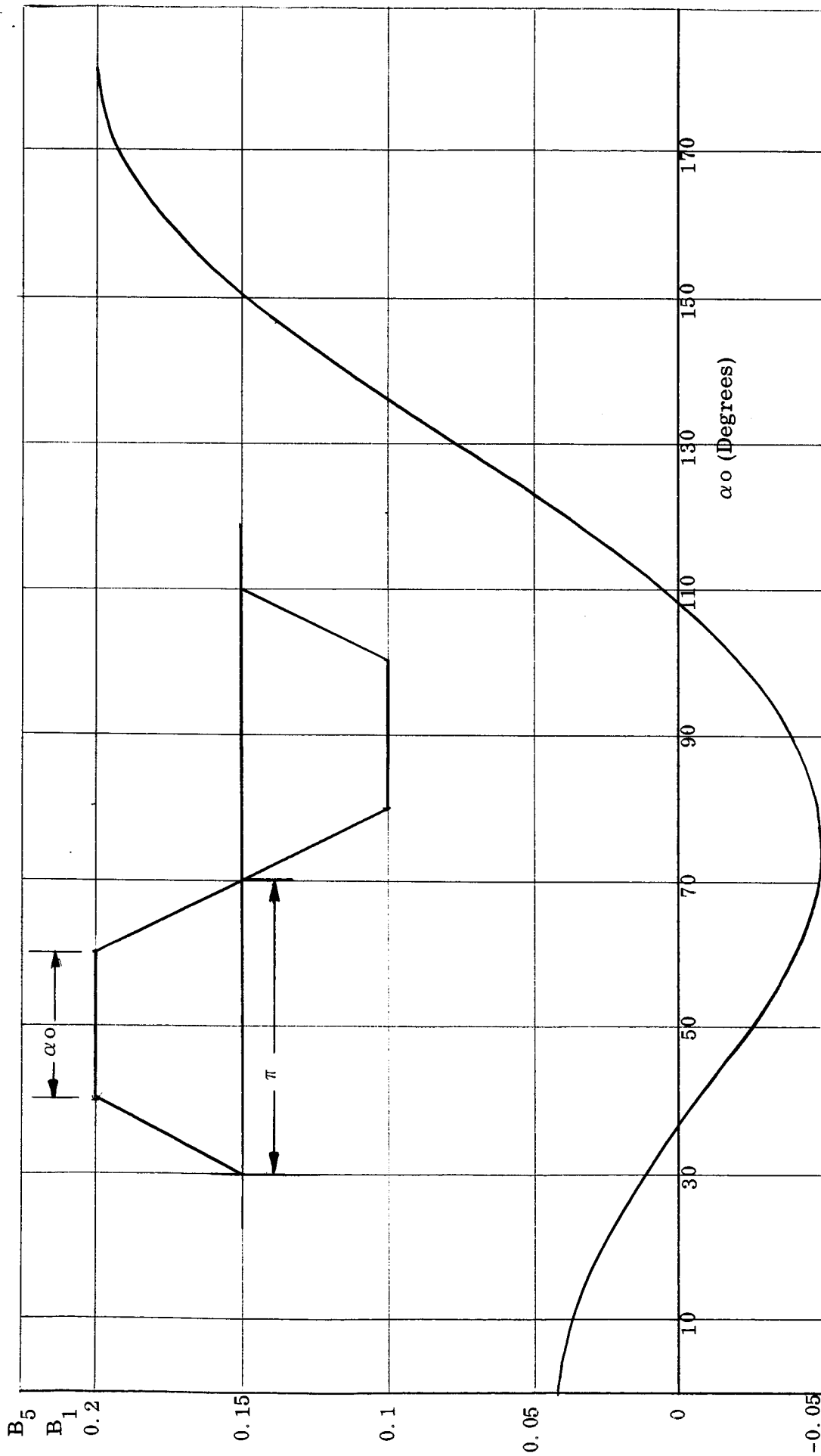

FIGURE A6
TRAPEZOIDAL WAVE

FIGURE A7

RATIO $\dfrac{B_5}{B_1}$ FOR TRAPEZOIDAL WAVE

The Fourier series for this wave is -

$$\text{(28)} \quad B(\alpha) = \frac{8B_o}{\pi^2 (1 - \frac{\alpha q}{\pi})} \sum_{n=1}^{\infty} \frac{\sin^2 n \frac{\pi}{2}}{n^2} \cos n \frac{\alpha o}{2} \cos n\alpha \quad \text{gauss}$$

where αo is the angular width of the wave at its peak. For this wave -

$$\text{(29)} \quad \frac{B_5}{B_1} = \frac{\cos \frac{5\alpha o}{2}}{25 \cos \frac{\alpha o}{2}}$$

a plot of this ratio is given in Figure 7. From this curve

$$\text{(30)} \quad \left. \frac{B_5}{B_1} \right|_{\text{max.}} = +.20 \quad \text{for } \alpha o = 180^O \text{ (square wave)}$$

$$\left. \frac{B_5}{B_1} \right|_{\text{min.}} = -.0495 \quad \text{for } \alpha o = 72^O$$

Comparing equations (27) with (30) it can be seen that there is no possibility of achieving a condition of reasonable slot utilization even with allowance for substantial error in the assumption of a trapezoidal flux wave. The conditions for a wye winding appear better than for a delta winding, but this is only for the very unlikely case of a true square wave flux distribution. It is, of course, possible to devise a winding which will result in a voltage with 7% fifth harmonic, but this can only be done at the cost of very poor winding efficiency.

CONCLUSIONS

The purpose of this analysis was to explore the possibility of constructing an armature winding which would produce a counter EMF wave form that is relatively flat over a 60 degree commutating zone. This zone width is associated with an armature having three terminal connections and three balanced phase windings.

It has been demonstrated that the terminal voltages of both delta and wye connected windings do not contain a third harmonic. This is the primary obstacle because the third harmonic is the major influence in wave flattening.

An attempt was made to utilize the fifth harmonic of flux as a means for flattening the terminal voltage wave. The results indicate that a typical flux wave does not contain a fifth harmonic of sufficient amplitude to permit a winding which uses the slot winding space efficiently. This was demonstrated only for an armature with 9 slots per pair of poles, but within conventional size limits this is the only practical number of slots which is suitable for a three phase winding and which contains coils that respond well to both the fundamental and fifth harmonics of flux.